Delft University of Technology

Adaptive Integral Sliding Mode Control in the Presence of State-Dependent Uncertainty

Li, Peng; Liu, Di; Baldi, Simone

Important note
To cite this publication, please use the final published version (if applicable).
Please check the document version above.

Adaptive Integral Sliding Mode Control in the Presence of State-Dependent Uncertainty

Peng Li [ID], Di Liu [ID], *Member, IEEE*, and Simone Baldi [ID], *Senior Member, IEEE*

Abstract—**Adaptive integral sliding mode control (AISMC) is an extension of adaptive sliding mode control which is a way to ensure sliding motion while handling system uncertainties. However, conventional AISMC formulations require to different extent *a priori* knowledge of the system uncertainty: either the upper bound of the uncertainty or of its time derivative are assumed to be bounded *a priori*, or the uncertainty is assumed to be parametrized by some structure-dependent factorization. This work proposes a variant of AISMC with reduced *a priori* knowledge of the system uncertainty: it is shown that Euler–Lagrange dynamics typical of sliding mode literature admit a structure-independent parametrization of the system uncertainty. This parametrization is not the result of structural knowledge, but it comes from basic properties of Euler–Lagrange dynamics, valid independently on the structure of the system. The AISMC control method arising from this parametrization is analyzed in the Lyapunov stability framework, and validated in systems with different structures: a surface vessel and an aerial vehicle.**

Index Terms—**Adaptive integral sliding mode, aerial vehicle, Euler-Lagrange dynamics, state-dependent uncertainty.**

I. INTRODUCTION

EULER–LAGRANGE (EL) dynamics can be used to describe many real-world systems such as aircrafts [1], manipulators [2], mobile robots [3], multiagent networks [4], and many more [5], [6]. In these and other applications, the dynamics of the system may be not known exactly, e.g., due to unmodeled dynamics [7], uncertain parameters [8]–[10], and parametric variations [11]–[13]. Control of EL systems in the presence of such uncertainties is still a challenging subject.

Robust control of uncertain EL systems based on sliding mode control (SMC) is one of the most popular methods to tackle uncertainties [14], [15]. The standard SMC for EL systems uses a proportional-derivative (PD) sliding surface and drives the system trajectories on the surface by using a sign function control action weighted by a fixed control gain. To avoid issues, such as chattering, the sliding surface can be replaced by a boundary layer by using a saturation function in place of the sign function. The control gain of the sign (or of the saturation) function should be as big as the upper bound of the uncertainties. Such prior knowledge about the bounds of system uncertainties represents a recognized drawback of SMC [16]. This has led to proposing adaptive sliding mode control (ASMC) methods where, instead of being fixed, the control gain of SMC is adapted online to cope with the uncertainties.

ASMC can be divided into three categories, depending on the way the control gain is adapted: monotonically increasing ASMC [17], equivalent control ASMC [18], and increasing/decreasing ASMC [19]. These methods assume that the uncertainties [20] or their time derivative [18] are upper bounded *a priori* by possibly unknown constants. Because uncertainties are in practice state dependent, assuming a constant upper bound is equivalent to assuming that the state is bounded before actually proving stability. Efforts in relaxing this restrictive assumption require structural knowledge of the system, e.g., linear-in-parameters [21], [22] or nonlinear [23] structure. For example, linear-in-parameters structure factorizes the uncertainty using a constant matrix and a known regressor: such a regressor takes a different form for aircrafts, manipulators, mobile robots, etc., and might even be unavailable.

Integral SMC (ISMC) [24] and PID-based SMC (PID-SMC) [25] are other improvements to the standard SMC. Both methods use a proportional-integral-derivative (PID) sliding surface, i.e., they bring the advantages of integral control in achieving smaller steady-state error [26]–[29]. It is worth noticing that ISMC and PID-SMC are very close to each other: since the 1980s, Slotine classified PID-SMC as an ISMC method [30], [31, Ch. 7], and the only difference between the two methods is that ISMC can choose the initial conditions to let the system trajectory start directly from the sliding surface. See also recent ISMC results using linear nominal dynamics perturbed by input nonlinearities [32], [33].

The combination of integral control and adaptation has been proposed under the name of adaptive integral sliding mode

control (AISMC) [15], [34], [35]. Unfortunately, also AISMC requires *a priori* bounded uncertainty [15], [27] or specific structural knowledge [34], [35]. Summarizing, control of EL systems with reduced knowledge of system uncertainties is largely open. In this article, we propose a novel AISMC method based on the following contributions:

1) the system uncertainty is not taken to be bounded *a priori* by a constant;
2) the state-dependent structure we propose is not the result of some structural knowledge, but it comes directly from basic properties of EL dynamics (valid independently on the structure of the system);
3) we show that the proposed AISMC framework provides a systematic way to enhance robustness and adaptation in PID-based loops.

Item a) is achieved by showing boundedness after the control design (a posteriori), rather than before the control design (*a priori*); item b) is achieved by deriving analytically an upper bound structure for the uncertainty solely based on properties of EL systems; and item c) derives from the structure of the proposed control law: note that the standard SMC (or recent advances [16]) cannot be systematically integrated in PID loops due to their lack of integral action. The structure-independent nature of the proposed method is tested in systems with different structures: a surface vessel case, and software-in-the-loop (SITL) experiments for an ArduPilot-based fixed-wing autopilot. The ArduPilot-based autopilot is based on PID control and thus provides an interesting test case for showing how the AISMC framework enhances PID-based loops.

This article is organized as follows. Section II gives the EL formulation. Section III covers control design and stability analysis. Validations are in Section IV. Finally, Section V concludes this article.

Notations: The sets of real numbers, positive real numbers, and real $n \times m$ matrices are denoted by $\mathbb{R}$, $\mathbb{R}^+$ and $\mathbb{R}^{n \times m}$, respectively; $\mathbb{I}_n$ is the $n \times n$ identity matrix; a bold notation is used for vectors, i.e., $\boldsymbol{\sigma} = [\sigma_1, \ldots, \sigma_n]^T$; $\|(\cdot)\|$ and $\lambda_{min}(\cdot)$ denote the Euclidean-norm and the minimum eigenvalue of $(\cdot)$, respectively.

II. SYSTEM DYNAMICS AND PROBLEM FORMULATION

Consider the class of Euler–Lagrange (EL) systems

$$\mathbf{M}(\mathbf{q})\ddot{\mathbf{q}} + \mathbf{C}(\mathbf{q}, \dot{\mathbf{q}})\dot{\mathbf{q}} + \mathbf{G}(\mathbf{q}) + \mathbf{F}(\dot{\mathbf{q}}) + \mathbf{d} = \mathbf{u} \qquad (1)$$

where $\mathbf{q} \in \mathbb{R}^n$ is the state vector, and $\dot{\mathbf{q}} \in \mathbb{R}^n$ is its time derivative; $\mathbf{M}(\mathbf{q}) \in \mathbb{R}^{n \times n}$ denotes the mass/inertia matrix; $\mathbf{C}(\mathbf{q}, \dot{\mathbf{q}}) \in \mathbb{R}^{n \times n}$ denotes the Coriolis term; $\mathbf{G}(\mathbf{q}) \in \mathbb{R}^n$ denotes the gravity term; $\mathbf{F}(\dot{\mathbf{q}}) \in \mathbb{R}^n$ denotes the damping and friction forces; $\mathbf{d} \in \mathbb{R}^n$ denotes bounded external disturbances and $\mathbf{u} \in \mathbb{R}^n$ is the control input.

For most real-world mechanical systems, the literature has shown that some properties hold for the EL terms in (1) (cf. [1], [16], [36]). These properties will be adopted for controller design and stability analysis.

Property 1: There exist $c_u, g_u, f_u, d_u \in \mathbb{R}^+$ such that $\|\mathbf{C}(\mathbf{q}, \dot{\mathbf{q}})\| \le c_u\|\dot{\mathbf{q}}\|$, $\|\mathbf{G}(\mathbf{q})\| \le g_u$, $\|\mathbf{F}(\dot{\mathbf{q}})\| \le f_u\|\dot{\mathbf{q}}\|$ and $\|\mathbf{d}(t)\| \le d_u$.

Property 2: Matrix $\mathbf{M}(\mathbf{q})$ is symmetric and uniformly positive, which implies that $\exists\, m_u, m_l \in \mathbb{R}^+$ such that

$$0 < m_l\mathbb{I}_n \le \mathbf{M}(\mathbf{q}) \le m_u\mathbb{I}_n. \qquad (2)$$

Property 3: Matrix $\dot{\mathbf{M}}(\mathbf{q}) - 2\mathbf{C}(\mathbf{q}, \dot{\mathbf{q}})$ is skew symmetric, i.e., $\mathbf{x}^T(\dot{\mathbf{M}}(\mathbf{q}) - 2\mathbf{C}(\mathbf{q}, \dot{\mathbf{q}}))\mathbf{x} = 0$ for any nonzero vector $\mathbf{x}$.

Remark 1 (Uncertainty of the dynamics): Properties 1–3 hold independently of the structure of the system: manipulators, aircrafts, mobile robots, etc., satisfy the bounds in Properties 1–3 for possibly unknown constants (cf. [1], [16], [36]). Throughout this work, $\mathbf{M}, \mathbf{C}, \mathbf{F}, \mathbf{G}, \mathbf{d}$ in (1) and $m_u, m_l, c_u, g_u, f_u, d_u$ in their bounds are considered to be unknown.

Denote $\mathbf{q}_d \in \mathbb{R}^n$ as the desired states, which satisfy $\|\dot{\mathbf{q}}_d(t)\| \le q_u, \forall t$ and $\|\ddot{\mathbf{q}}_d(t)\| \le q_{uu}\, \forall t$. The following question arises.

Problem: Find a control strategy $\mathbf{u}(\cdot)$ such that the solutions of the EL system (1) track the desired states $\mathbf{q}_d$, in the presence of uncertainty of the dynamics as in Remark 1.

In the following, we will illustrate the derivation process of the system uncertainty for two kinds of sliding surface: the first one is commonly referred to as PID-based sliding mode control (PID-SMC [25]); the other one is commonly refereed to as integral sliding mode control (ISMC [24]). As detailed in [30], [31, Ch. 7], the main difference between the two methods is a particular choice of the initial conditions.

A. Uncertainty Structure for PID-Based Sliding Surface

Let $\mathbf{e}(t) = \mathbf{q}_d(t) - \mathbf{q}(t)$ be the tracking error. The PID sliding variable $\boldsymbol{\sigma}_1$ is defined in the literature as

$$\boldsymbol{\sigma}_1(t) \triangleq \dot{\mathbf{e}}(t) + \boldsymbol{\Gamma}_1\mathbf{e}(t) + \boldsymbol{\Gamma}_2\int_0^t \mathbf{e}(\tau)d\tau \qquad (3)$$

where $\boldsymbol{\Gamma}_1, \boldsymbol{\Gamma}_2 \in \mathbb{R}^{n \times n}$ are positive definite matrices. Take the time derivative of (3) and multiply by $\mathbf{M}$. Using (1), we obtain (time and state dependence are omitted for compactness)

$$\mathbf{M}\dot{\boldsymbol{\sigma}}_1 = \mathbf{M}(\ddot{\mathbf{q}}_d - \ddot{\mathbf{q}} + \boldsymbol{\Gamma}_1\dot{\mathbf{e}} + \boldsymbol{\Gamma}_2\mathbf{e})$$
$$= -\mathbf{u} - \mathbf{C}\boldsymbol{\sigma}_1 + \boldsymbol{\delta}_1 \qquad (4)$$

where

$$\boldsymbol{\delta}_1 \triangleq \mathbf{C}\dot{\mathbf{q}} + \mathbf{G} + \mathbf{F} + \mathbf{d}$$
$$+ \mathbf{M}\ddot{\mathbf{q}}_d + \mathbf{M}\boldsymbol{\Gamma}_1\dot{\mathbf{e}} + \mathbf{M}\boldsymbol{\Gamma}_2\mathbf{e} + \mathbf{C}\boldsymbol{\sigma}_1 \qquad (5)$$

represents an aggregate state-dependent uncertainty. Next, we aim to find an appropriate (state-dependent) bound for such uncertainty. By combining (3) and Properties 1 and 2, we obtain

$$\|\boldsymbol{\delta}_1\| \le c_u\|\dot{\mathbf{q}}\|^2 + g_u + f_u\|\dot{\mathbf{q}}\| + d_u$$
$$+ m_u(\|\ddot{\mathbf{q}}_d\| + \|\boldsymbol{\Gamma}_1\|\|\dot{\mathbf{e}}\| + \|\boldsymbol{\Gamma}_2\|\|\mathbf{e}\|)$$
$$+ c_u\|\dot{\mathbf{q}}\|(\|\dot{\mathbf{e}}\| + \|\boldsymbol{\Gamma}_1\|\|\mathbf{e}\| + \|\boldsymbol{\Gamma}_2\|\|\int_0^t \mathbf{e}(\tau)d\tau\|). \qquad (6)$$

Take

$$\boldsymbol{\xi}(t) = \begin{bmatrix} \mathbf{e}^T(t) & \dot{\mathbf{e}}^T(t) & (\int_0^t \mathbf{e}(\tau)d\tau)^T \end{bmatrix}^T.$$

Then, the following inequalities hold:

$$\|\boldsymbol{\xi}(t)\| \geq \|\mathbf{e}(t)\|, \quad \|\boldsymbol{\xi}(t)\| \geq \|\dot{\mathbf{e}}(t)\|$$
$$\|\boldsymbol{\xi}(t)\| \geq \| \int_0^t \mathbf{e}(\tau)d\tau\|. \tag{7}$$

Using these inequalities and substituting $\dot{\mathbf{q}} = -\dot{\mathbf{e}} + \dot{\mathbf{q}}_d$ into (6), we have

$$\|\boldsymbol{\delta}_1\| \leq \kappa_0^* + \kappa_1^*\|\boldsymbol{\xi}(t)\| + \kappa_2^*\|\boldsymbol{\xi}(t)\|^2 \tag{8}$$

where $\kappa_0^*, \kappa_1^*, \kappa_2^*$ are unknown positive constants defined as

$$\kappa_0^* \triangleq c_u q_u^2 + g_u + f_u q_u + d_u + m_u q_{uu}$$
$$\kappa_1^* \triangleq c_u q_u (3 + \|\boldsymbol{\Gamma}_1\| + \|\boldsymbol{\Gamma}_2\|) + f_u$$
$$+ m_u(\|\boldsymbol{\Gamma}_1\| + \|\boldsymbol{\Gamma}_2\|) \tag{9}$$
$$\kappa_2^* \triangleq c_u(2 + \|\boldsymbol{\Gamma}_1\| + \|\boldsymbol{\Gamma}_2\|).$$

B. Uncertainty Structure for Integral Sliding Surface

The integral sliding variable $\boldsymbol{\sigma}_2$ is defined in literature as

$$\boldsymbol{\sigma}_2(t) \triangleq \dot{\mathbf{e}}(t) + \boldsymbol{\Omega}_1 \mathbf{e}(t)$$
$$+ \boldsymbol{\Omega}_2 \int_0^t \mathbf{e}(\tau)d\tau - \dot{\mathbf{e}}(0) - \boldsymbol{\Omega}_1 \mathbf{e}(0) \tag{10}$$

where $\boldsymbol{\Omega}_1, \boldsymbol{\Omega}_2 \in \mathbb{R}^{n \times n}$ are positive definite matrices. It is worth noticing that the main difference with (3) are the initial conditions $\mathbf{e}(0)$, $\dot{\mathbf{e}}(0)$, which allow $\boldsymbol{\sigma}_2(0) = 0$, i.e., the system starts from the sliding surface. Even for the sliding surface (10), an appropriate (state-dependent) upper bound structure for the uncertainty will be derived. Take the time derivative of (10) and multiply by $\mathbf{M}$. Using (1), we can obtain

$$\mathbf{M}\dot{\boldsymbol{\sigma}}_2 = \mathbf{M}(\ddot{\mathbf{q}}_d - \ddot{\mathbf{q}} + \boldsymbol{\Omega}_1\dot{\mathbf{e}} + \boldsymbol{\Omega}_2\mathbf{e})$$
$$= -\mathbf{u} - \mathbf{C}\boldsymbol{\sigma}_2 + \boldsymbol{\delta}_2 \tag{11}$$

where

$$\boldsymbol{\delta}_2 \triangleq \mathbf{C}\dot{\mathbf{q}} + \mathbf{G} + \mathbf{F} + \mathbf{d}$$
$$+ \mathbf{M}\ddot{\mathbf{q}}_d + \mathbf{M}\boldsymbol{\Omega}_1\dot{\mathbf{e}} + \mathbf{M}\boldsymbol{\Omega}_2\mathbf{e} + \mathbf{C}\boldsymbol{\sigma}_2. \tag{12}$$

Combining (10) and Properties 1 and 2, we obtain the upper bound

$$\|\boldsymbol{\delta}_2\| \leq c_u\|\dot{\mathbf{q}}\|^2 + g_u + f_u\|\dot{\mathbf{q}}\| + d_u$$
$$+ m_u(\|\ddot{\mathbf{q}}_d\| + \|\boldsymbol{\Omega}_1\|\|\dot{\mathbf{e}}\| + \|\boldsymbol{\Omega}_2\|\|\mathbf{e}\|)$$
$$+ c_u\|\dot{\mathbf{q}}\|(\|\dot{\mathbf{e}}\| + \|\boldsymbol{\Omega}_1\|\|\mathbf{e}\| + \|\boldsymbol{\Omega}_2\|\| \int_0^t \mathbf{e}(\tau)d\tau\|$$
$$+ \|\dot{\mathbf{e}}(0)\| + \|\boldsymbol{\Omega}_1\|\|\mathbf{e}(0)\|). \tag{13}$$

Using (7) and substituting $\dot{\mathbf{q}} = -\dot{\mathbf{e}} + \dot{\mathbf{q}}_d$ into (13), we have

$$\|\boldsymbol{\delta}_2\| \leq \nu_0^* + \nu_1^*\|\boldsymbol{\xi}(t)\| + \nu_2^*\|\boldsymbol{\xi}(t)\|^2 \tag{14}$$

where $\nu_0^*, \nu_1^*, \nu_2^*$ are unknown positive constants defined as

$$\nu_0^* \triangleq c_u q_u^2 + g_u + f_u q_u + d_u + m_u q_{uu}$$
$$+ c_u q_u(\|\dot{\mathbf{e}}(0)\| + \|\boldsymbol{\Omega}_1\|\|\mathbf{e}(0)\|)$$
$$\nu_1^* \triangleq c_u\|\dot{\mathbf{q}}_d\|(3 + \|\boldsymbol{\Omega}_1\| + \|\boldsymbol{\Omega}_2\|) + f_u + m_u(\|\boldsymbol{\Omega}_1\| \tag{15}$$
$$+ \|\boldsymbol{\Omega}_2\|) + c_u(\|\dot{\mathbf{e}}(0)\| + \|\boldsymbol{\Omega}_1\|\|\mathbf{e}(0)\|)$$
$$\nu_2^* \triangleq c_u(2 + \|\boldsymbol{\Omega}_1\| + \|\boldsymbol{\Omega}_2\|).$$

We have derived that both sliding surfaces $\boldsymbol{\sigma}_1(\cdot)$ and $\boldsymbol{\sigma}_2(\cdot)$ share a similar upper bound structure as (8) and (14). Therefore, in the following, we will analyze our proposed adaptive integral sliding mode control (AISMC) method by simply using $\boldsymbol{\sigma}(\cdot)$ to denote either $\boldsymbol{\sigma}_1(\cdot)$ or $\boldsymbol{\sigma}_2(\cdot)$. Accordingly, we use

$$\mathbf{M}\dot{\boldsymbol{\sigma}} = -\mathbf{u} - \mathbf{C}\boldsymbol{\sigma} + \boldsymbol{\delta} \tag{16}$$

$$\|\boldsymbol{\delta}\| \leq \theta_0^* + \theta_1^*\|\boldsymbol{\xi}\| + \theta_2^*\|\boldsymbol{\xi}\|^2 \tag{17}$$

that is, θ_i^* denotes either κ_i^* in (8) or ν_i^* in (14), and $\boldsymbol{\delta}$ denotes either $\boldsymbol{\delta}_1$ in (8) or $\boldsymbol{\delta}_2$ in (14). For both sliding surfaces, we will refer to the proposed method simply as AISMC.

Remark 2 (No structural knowledge): The state-dependent structure (17) is not the result of structural knowledge, but comes directly from the basic Properties 1–3 of EL dynamics, which are valid independently on the structure of the system.

Remark 3 (Bounded stability): Of the three families of ASMC proposed in the literature (monotonically increasing ASMC [17], equivalent control ASMC [18], and increasing/decreasing ASMC [19]), the last two attain globally uniformly ultimately boundedness (GUUB). Only the first one can achieve asymptotic tracking, provided a sign function is used in the control. However, a sign function with monotonically increasing gain can lead to undesirable chattering behavior with large amplitude. This work will study stability in the sense of GUUB, in line with the stability results of most ASMC designs.

Definition 1: (GUUB) Consider a signal $\boldsymbol{\sigma}(\cdot)$. Assume there exists $\vartheta_a, \vartheta_c > 0$ and for every $0 < \vartheta_a < \vartheta_c$ there exists $T \geq 0$ and $\vartheta > 0$ such that $\|\boldsymbol{\sigma}(t_0)\| \leq \vartheta_a$ implies

$$\|\boldsymbol{\sigma}(t)\| \leq \vartheta \quad \forall t \geq t_0 + T \tag{18}$$

and ϑ_a can be arbitrarily large. Then, the signal $\boldsymbol{\sigma}(\cdot)$ is called global uniformly ultimately bounded with ultimate bound ϑ.

The following is a Lyapunov characterization of GUUB, adopted from [37, Ch. 4].

Lemma 1: Let V be a continuously differentiable function such that

$$c_1\|\boldsymbol{\sigma}\|^2 \leq V(\boldsymbol{\sigma}) \leq c_2\|\boldsymbol{\sigma}\|^2$$
$$\dot{V}(\boldsymbol{\sigma}) \leq -c_3 V(\boldsymbol{\sigma}) \quad \forall\|\boldsymbol{\sigma}\| \geq \mu \tag{19}$$

with $c_1, c_2, c_3 > 0$. Take a ball $\mathcal{B}_r$ of radius r and let

$$\mu \leq r\left(\frac{c_1}{c_2}\right)^{1/2}. \tag{20}$$

Define $\vartheta_a \triangleq r(c_1/c_2)^{1/2}$. Then, for every initial state $\boldsymbol{\sigma}(t_0)$ satisfying $\|\boldsymbol{\sigma}(t_0)\|^2 \leq \vartheta_a$ there is $T \geq 0$ such that (18) holds with $\vartheta \triangleq \mu(c_2/c_1)^{1/2}$ and ϑ_a can be arbitrarily large.
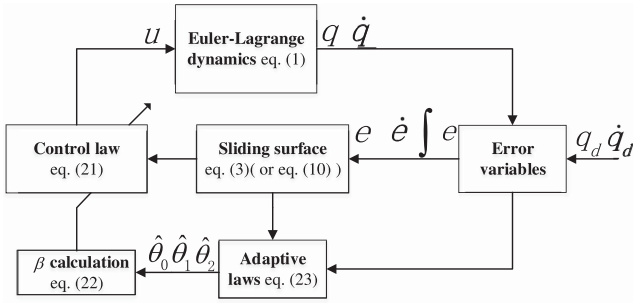
Fig. 1.   Block diagram of the proposed control framework.

III. AISMC DESIGN AND STABILITY ANALYSIS

To tackle the uncertainty (17), we propose the control law

$$\mathbf{u}(t) = \mathbf{\Upsilon}\boldsymbol{\sigma}(t) + \beta(t)\operatorname{sat}(\boldsymbol{\sigma}(t)/\epsilon) \qquad (21)$$

where $\mathbf{\Upsilon}$ is a positive definite matrix, ϵ is a designed scalar, $\operatorname{sat}(x)$ is the saturation function

$$\operatorname{sat}(x) = \begin{cases} x & \text{if } -1 < x < 1 \\ \operatorname{sign}(x) & \text{else} \end{cases}$$

and

$$\beta(t) = \hat{\theta}_0(t) + \hat{\theta}_1(t)\|\boldsymbol{\xi}(t)\| + \hat{\theta}_2(t)\|\boldsymbol{\xi}(t)\|^2. \qquad (22)$$

The gains $\hat{\theta}_i$ (for $i = 0, 1, 2$) in (22) are the estimates of the constants θ_i^* in (17). These gains are updated according to the following adaptive laws:

$$\dot{\hat{\theta}}_i(t) = \eta_i\|\boldsymbol{\sigma}(t)\|\|\boldsymbol{\xi}(t)\|^i - \alpha_i\eta_i\hat{\theta}_i(t) \qquad (23)$$

where η_i, α_i ($i = 0, 1, 2$) are positive gains, and the initial conditions satisfy $\hat{\theta}_i(0) > 0$.

For the proposed control framework summarized in Fig. 1, the following stability result holds.

Theorem 1: The trajectories of the EL dynamics (1) with Properties 1–3, implementing the control law (21) and (22), with adaptive law (23), are GUUB, and an ultimate bound ϑ on $\boldsymbol{\sigma}$ is given by

$$\vartheta = \sqrt{\frac{\sum_{i=0}^{2} \alpha_i\theta_i^{*2}}{m_l(\varsigma - \omega)}} \qquad (24)$$

where $\varsigma \triangleq \frac{\min_i\{\lambda_{min}(\mathbf{\Upsilon}), \alpha_i/2\}}{\max\{m_u/2, 1/2\eta_i\}} > 0$, and $0 < \omega < \varsigma$.

Proof: Take the integral of the adaptive law (23) from 0 to t

$$\hat{\theta}_i(t) = e^{-\alpha_i\eta_i t}\hat{\theta}_i(0)$$

$$+ \int_0^t e^{-\alpha_i(t-\tau)\eta_i}\|\boldsymbol{\sigma}(t)\|\|\boldsymbol{\xi}(t)\|^i \eta_i d\tau. \qquad (25)$$

Since $\hat{\theta}_i(0) > 0$ and $\|\boldsymbol{\sigma}(t)\|\|\boldsymbol{\xi}(t)\|^i$ is positive, we obtain

$$\hat{\theta}_i(t) \geq 0 \quad \forall t \geq 0. \qquad (26)$$

Closed-loop stability is analyzed via the Lyapunov function

$$V = \frac{1}{2}\boldsymbol{\sigma}^T\mathbf{M}\boldsymbol{\sigma} + \sum_{i=0}^{2} \frac{1}{2\eta_i}(\theta_i^* - \hat{\theta}_i)^2. \qquad (27)$$

Using (16), (21), and Property 3, we get the time derivative

$$\dot{V} = \boldsymbol{\sigma}^T(-\mathbf{u} - \mathbf{C}\boldsymbol{\sigma} + \boldsymbol{\delta}) + \frac{1}{2}\boldsymbol{\sigma}^T\dot{\mathbf{M}}\boldsymbol{\sigma} + \sum_{i=0}^{2}(\hat{\theta}_i - \theta_i^*)\dot{\hat{\theta}}_i/\eta_i$$

$$= \boldsymbol{\sigma}^T(-\mathbf{\Upsilon}\boldsymbol{\sigma} - \beta\operatorname{sat}(\boldsymbol{\sigma}/\epsilon) + \boldsymbol{\delta})$$

$$+ \frac{1}{2}\boldsymbol{\sigma}^T(\dot{\mathbf{M}} - 2\mathbf{C})\boldsymbol{\sigma} + \sum_{i=0}^{2}(\hat{\theta}_i - \theta_i^*)\dot{\hat{\theta}}_i/\eta_i$$

$$= \boldsymbol{\sigma}^T(-\mathbf{\Upsilon}\boldsymbol{\sigma} - \beta\operatorname{sat}(\boldsymbol{\sigma}/\epsilon) + \boldsymbol{\delta}) + \sum_{i=0}^{2}(\hat{\theta}_i - \theta_i^*)\dot{\hat{\theta}}_i/\eta_i. \qquad (28)$$

Then, using (17) and the fact that $\beta \geq 0$ from (26), we have

$$\dot{V} \leq -\boldsymbol{\sigma}^T\mathbf{\Upsilon}\boldsymbol{\sigma} - \sum_{i=0}^{2}(\hat{\theta}_i - \theta_i^*)(\|\boldsymbol{\xi}\|^i\|\boldsymbol{\sigma}\| - \dot{\hat{\theta}}_i/\eta_i). \qquad (29)$$

Using (23) yields

$$(\hat{\theta}_i - \theta_i^*)\dot{\hat{\theta}}_i/\eta_i = \|\boldsymbol{\sigma}\|(\hat{\theta}_i - \theta_i^*)\|\boldsymbol{\xi}\|^i + \alpha_i\hat{\theta}_i\theta_i^* - \alpha_i\hat{\theta}_i^2. \qquad (30)$$

Substituting (30) into (29) gives

$$\dot{V} \leq -\lambda_{min}(\mathbf{\Upsilon})\|\boldsymbol{\sigma}\|^2 + \sum_{i=0}^{2}(\alpha_i\hat{\theta}_i\theta_i^* - \alpha_i\hat{\theta}_i^2)$$

$$\leq -\lambda_{min}(\mathbf{\Upsilon})\|\boldsymbol{\sigma}\|^2 - \sum_{i=0}^{2}\frac{\alpha_i}{2}((\hat{\theta}_i - \theta_i^*)^2 - \theta_i^{*2}) \qquad (31)$$

where we have used the inequality

$$\hat{\theta}_i\theta_i^* - \hat{\theta}_i^2 = -\left(\frac{\hat{\theta}_i}{\sqrt{2}} - \frac{\theta_i^*}{\sqrt{2}}\right)^2 + \frac{\theta_i^{*2}}{2} - \frac{\hat{\theta}_i^2}{2}$$

$$\leq -\left(\frac{\hat{\theta}_i}{\sqrt{2}} - \frac{\theta_i^*}{\sqrt{2}}\right)^2 + \frac{\theta_i^{*2}}{2}.$$

From Lyapunov function (27), we have

$$V \leq \frac{m_u}{2}\|\boldsymbol{\sigma}\|^2 + \sum_{i=0}^{2}\frac{1}{2\eta_i}(\hat{\theta}_i - \theta_i^*)^2 \qquad (32)$$

and substituting (32) into (31) gives

$$\dot{V} \leq -\varsigma V + \frac{1}{2}\sum_{i=0}^{2}\alpha_i\theta_i^{*2} \qquad (33)$$

where $\varsigma \triangleq \frac{\min_i\{\lambda_{min}(\mathbf{\Upsilon}), \alpha_i/2\}}{\max_i\{m_u/2, 1/2\eta_i\}} > 0$. Select a scalar $0 < \omega < \varsigma$, $\dot{V}$ can be further simplified as

$$\dot{V} \leq -\omega V - (\varsigma - \omega)V + \frac{1}{2}\sum_{i=0}^{2}\alpha_i\theta_i^{*2}. \qquad (34)$$

Define a scalar $\Theta \triangleq \frac{\sum_{i=0}^{2}\alpha_i\theta_i^{*2}}{2(\varsigma - \omega)}$ such that, if $V \geq \Theta$, then $\dot{V}(t) \leq -\omega V$. This is indeed the Lyapunov characterization of GUUB in Lemma 1 [37, Ch. 4]. We conclude that

$$V \leq \max\{V(0), \Theta\} \qquad \forall t \geq 0$$

and that V enters inside the ball Θ exponentially in finite time and stays therein for all future time [37, Sec. 4.8]. From the Lyapunov function (27) we have $V \geq (m_l/2)\|\boldsymbol{\sigma}\|^2$, which can be used to obtain the ultimate bound (24) on $\boldsymbol{\sigma}$. This bound is global and uniform as it is independent on initial conditions.

Remark 4 (Difference with standard ISMC): The term (22) can estimate the state-dependent bound of uncertainty without requiring structural knowledge of the system: this marks a major difference with standard ISMC [26], [27], or standard AISMC [15], [34], [35].

Remark 5 (PID structure): The proposed control (21) with PID-based sliding surface $\boldsymbol{\sigma}_1(t)$ in (3) can be viewed as a PID loop with embedded adaptation. More specifically, the control (21) comprises a standard PID action $\boldsymbol{\Upsilon}\boldsymbol{\sigma}_1(t)$ and an adaptive action $\beta(t)$ for the sliding mode term $\text{sat}(\boldsymbol{\sigma}_1(t)/\epsilon)$.

IV. VALIDATION EXPERIMENTS

To evaluate the effectiveness of the proposed framework, we consider two test cases with different system structures: a surface vessel test case, and a fixed-wing unmanned aerial vehicle (UAV) test case. A standard ISMC is used to compare the proposed method

$$\mathbf{u}(t) = \boldsymbol{\Upsilon}\boldsymbol{\sigma}(t) + \overline{\beta}\,\text{sat}(\boldsymbol{\sigma}(t)/\epsilon) \tag{35}$$

the main difference between the AISMC (21) and the standard ISMC (35) is the upper bound structure $\overline{\beta}$, which is a constant instead of changing online in an adaptive way.

A. Surface Vessel Test Case

To illustrate the performance of the proposed controller with integral sliding surface $\boldsymbol{\sigma}_2$ as in (10), consider the simplified dynamics of a surface vehicle as in [31, Ch. 7]

$$\begin{cases} \dot{q}_1 = q_2 \\ \dot{q}_2 = -cq_2|q_2|/m + u/m + d(t) \end{cases} \tag{36}$$

where q_1 and q_2 are position and speed of the vehicle, respectively; u is the control input, m is the mass of vehicle, and c is the friction coefficient. As explained in [31, Ch. 7], m and c are subject to uncertainty in practice. For simulations, we set $\mathbf{q}(0) = [-1, 0]^T$ and we consider a combination of the following uncertainty scenarios. For the uncertain mass:
1) $\mathcal{M}_0$: constant unknown mass $m = 3$;
2) $\mathcal{M}_1$: unknown mass changes $m = 3 \rightarrow 5$ at $t = 3$ s and $m = 5 \rightarrow 1$ at $t = 5$ s.

For the uncertain disturbance and friction:
1) $\mathcal{D}_0$: unknown $c(t) = 1.2 + 0.2\sin(|q_2|t)$, $d(t) = 3\sin(\pi t)$;
2) $\mathcal{D}_1$: unknown $c(t) = 1.2 + 0.4\sin(|q_2|t)$, $d(t) = 6\sin(\pi t)$;
3) $\mathcal{D}_2$: unknown $c(t) = 1.2 + 0.2|q_2|n(t)$, $d(t) = 3\sin(\pi t)$;
4) $\mathcal{D}_3$: unknown $c(t) = 1.2 + 0.4|q_2|n(t)$, $d(t) = 6\sin(\pi t)$;

where $n(t)$ represents a random noise uniformly distributed between -1 and 1. The term "unknown" denotes the fact that the value of the mass, of the disturbance and of the friction are not available for control design. By combining the situations above, we obtain eight scenarios, which are also reported in

Table I. Note that the sinusoidal friction was proposed in [31, Ex. 7.4], whereas the noise friction is further introduced for additional comparisons: also, cases $\mathcal{M}_1$, $\mathcal{D}_1$, $\mathcal{D}_2$, and $\mathcal{D}_3$ have been designed explicitly to test the capabilities of the controllers to cope with larger uncertainty.

The desired trajectory $\mathbf{q}_d$ is also taken from [31, Sec. 7]: it includes constant acceleration $\dot{q}_{d2} = 2$ m/s² at $t \in [0, 2)$s, constant velocity $q_{d2} = 4$m/s at $t \in [2, 4)$s, and constant acceleration $\dot{q}_{d2} = -2$m/s at $t \in [4, 6)$s. To construct the proposed AISMC in (21) and (10), we set $\boldsymbol{\Omega}_1 = 5.5, \boldsymbol{\Omega}_2 = 12, \mathbf{e}(0) = [1, 0]^T$, $\boldsymbol{\Upsilon} = 50$, and $\epsilon = 0.001$. In addition, we set $\eta = 385, \alpha_0 = 10^{-5}, \alpha_1 = 250, \alpha_2 = 175$ for the adaptive law in (23). Simulation are carried out using ode45 function in MATLAB with maximum step size 0.1 ms.

For comparison purposes, the standard ISMC as in (35) is used with $\overline{\beta} = 15$ or $\overline{\beta} = 25$. For compactness, tracking performance, tracking error, and control input are reported in Figs. 2 and 3 only for the first two scenarios of Table I. Figs. 2(a) and 3(a) display the position tracking error for the proposed AISMC and the standard ISMC with $\overline{\beta} = 15$ or $\overline{\beta} = 25$, under constant mass [see Fig. 2(a)] or mass change [see Fig. 3(a)]. For all tracking transients arising at $t = 2$, $t = 3$ and $t = 4$ s, the proposed AISMC gives a more accurate performance when compared to the standard ISMC. This becomes evident from the error norms $\|e\|$ reported in Figs. 2(b) and 3(b), which show that the proposed AISMC method has better tracking error with a reasonable control effort.

Table I reports the tracking error costs for all eight scenarios: the improvements of AISMC are consistent in all scenarios for both types of friction. Most importantly, as compared to ISMC, the proposed AISMC gives better percentage performance as more and more uncertainty affects the system: the percentage degradation of ISMC increases from +10.9% to +30.2% ($\overline{\beta} = 15$), and from +2% to +13.3% ($\overline{\beta} = 25$). This suggests that the proposed AISMC can automatically adapt its gain to the uncertainty situation, whereas the gain $\overline{\beta}$ of ISMC should be tuned appropriately.

B. UAV Test Case

The proposed AISMC with PID-based sliding surface $\boldsymbol{\sigma}_1$ (3) is tested in SITL environment for an ArduPilot-based autopilot for fixed-wing UAV. Using the state variables in Table II, the 6-DOF motion equations of the UAV are expressed as [38]

$$\begin{pmatrix} \dot{p}_n \\ \dot{p}_e \\ \dot{p}_d \end{pmatrix} = \boldsymbol{\mathcal{R}}_b^v(\phi, \theta, \psi) \begin{pmatrix} u_a \\ v_a \\ w_a \end{pmatrix} + \begin{pmatrix} w_n \\ w_e \\ w_d \end{pmatrix} \tag{37a}$$

$$\begin{pmatrix} \dot{u}_a \\ \dot{v}_a \\ \dot{w}_a \end{pmatrix} = \begin{pmatrix} rv_a - qw_a \\ pw_a - ru_a \\ qu_a - pv_a \end{pmatrix} + \frac{1}{m_a} \begin{pmatrix} f_x \\ f_y \\ f_z \end{pmatrix} - \boldsymbol{\mathcal{R}}_b^v(\phi, \theta, \psi) \begin{pmatrix} \dot{w}_n \\ \dot{w}_e \\ \dot{w}_d \end{pmatrix} \tag{37b}$$

$$\begin{pmatrix} \dot{\phi} \\ \dot{\theta} \\ \dot{\psi} \end{pmatrix} = \begin{pmatrix} 1 & s_\phi s_\theta/c_\theta & c_\phi s_\theta/c_\theta \\ 0 & c_\phi & -s_\phi \\ 0 & s_\phi/c_\theta & c_\phi/c_\theta \end{pmatrix} \begin{pmatrix} p \\ q \\ r \end{pmatrix} \tag{37c}$$
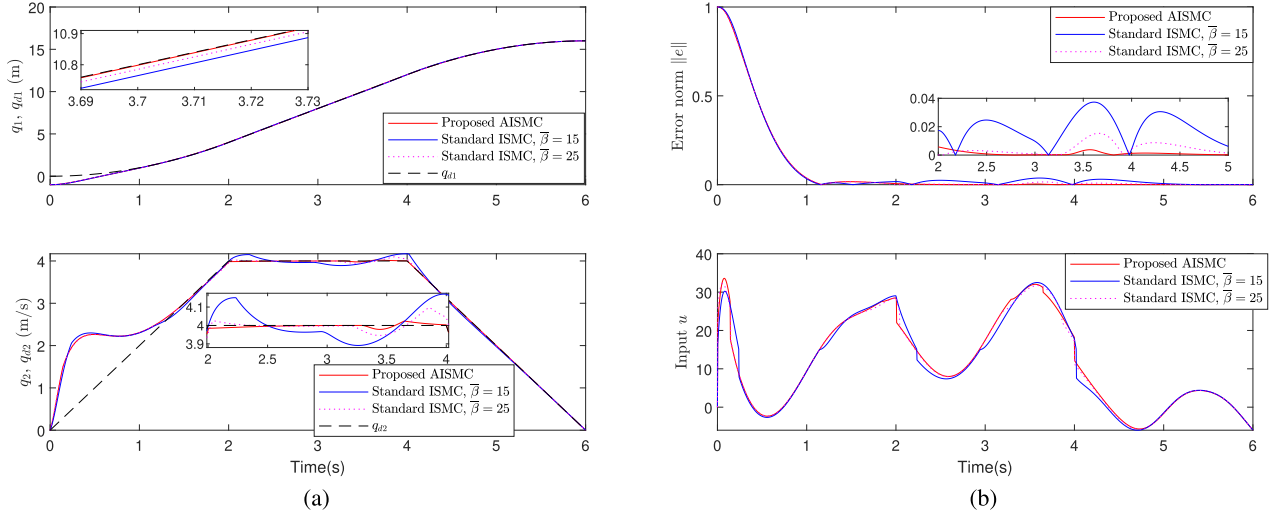
Fig. 2. Surface vessel with constant (unknown) mass $m = 3$. (a) Tracking performance for position and velocity. (b) Norm of the tracking error and control input.
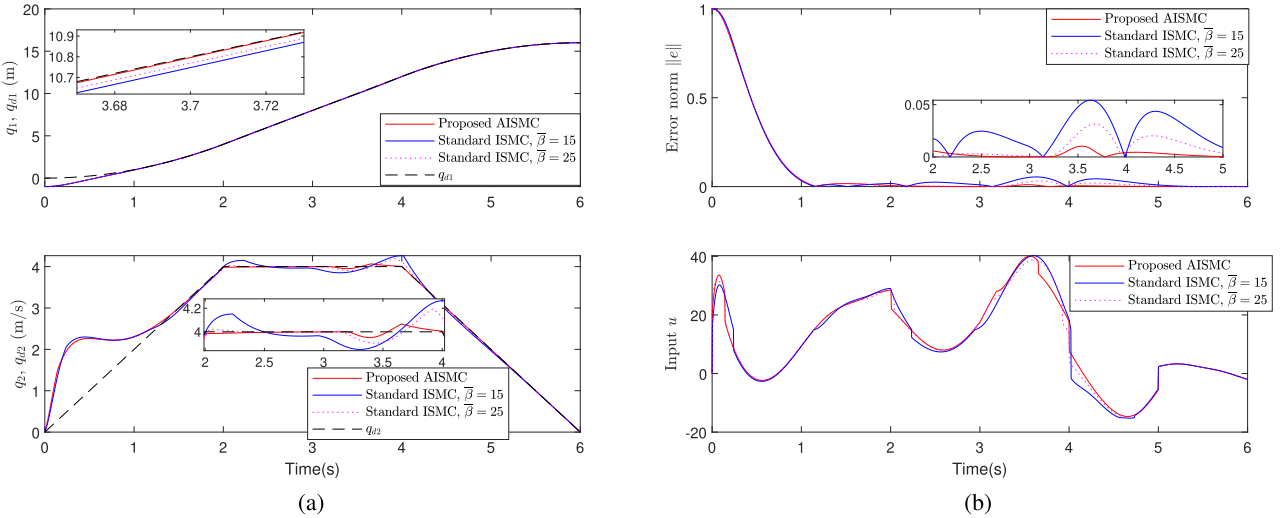

Fig. 3. Surface vessel with (unknown) mass changes $m = 3 \to 5$ at $t = 3$ s and $m = 5 \to 1$ at $t = 5$ s. (a) Tracking performance for position and velocity. (b) Norm of the tracking error and control input.

$$\begin{pmatrix} \dot{p} \\ \dot{q} \\ \dot{r} \end{pmatrix} = \begin{pmatrix} \Gamma_1 pq - \Gamma_2 qr \\ \Gamma_5 pr - \Gamma_6(p^2 - r^2) \\ \Gamma_7 pq - \Gamma_1 qr \end{pmatrix} + \begin{pmatrix} \Gamma_3 l + \Gamma_4 n \\ \frac{1}{J_y} m \\ \Gamma_4 l + \Gamma_8 n \end{pmatrix} \quad (37d)$$

with body-to-vehicle frame rotation matrix

$$\mathcal{R}_b^v(\phi, \theta, \psi) = (\mathcal{R}_v^b)^T(\phi, \theta, \psi)$$

$$= \begin{pmatrix} c_\theta c_\psi & s_\phi s_\theta c_\psi - c_\phi s_\psi & c_\phi s_\theta c_\psi + s_\phi s_\psi \\ c_\theta s_\psi & s_\phi s_\theta s_\psi + c_\phi c_\psi & c_\phi s_\theta s_\psi - s_\phi c_\psi \\ -s_\theta & s_\phi c_\theta & c_\phi c_\theta \end{pmatrix}$$

where m_a is the mass of UAV, w_n, w_e, w_d are the wind components, f_x, f_y, f_z are the forces exerted on the UAV in terms of its body frame, l, m, n denote the three components of the moments about the i^b, j^b, k^b axes, $\Gamma_1 \sim \Gamma_8$ and J_y are inertia terms. We

used the short notations $c_x \triangleq \cos x$ and $s_x \triangleq \sin x$. More details about (37) can be found in the literature, such as [38, Ch. 3].

The aerodynamic forces and moments can be decomposed into longitudinal and lateral. Longitudinal aerodynamics include lift force F_{lift}, drag force F_{drag}, and pitching moment m: they can be expressed to be dependent on the angle of attack α, pitch rate q and elevator angle δ_e as

$$F_{lift} = \frac{1}{2}\rho V_a^2 S C_L(\alpha, q, \delta_e) \quad (38a)$$

$$F_{drag} = \frac{1}{2}\rho V_a^2 S C_D(\alpha, q, \delta_e) \quad (38b)$$

$$m = \frac{1}{2}\rho V_a^2 S c C_m(\alpha, q, \delta_e) \quad (38c)$$

TABLE I
SURFACE VESSEL: TRACKING ERROR COSTS (POSITION AND VELOCITY) FOR PROPOSED AISMC AND STANDARD ISMC

Scenarios	Position error e costs		
	proposed AISMC	standard ISMC ($\bar{\beta} = 15$)	standard ISMC ($\bar{\beta} = 25$)
$\mathcal{M}_0, \mathcal{D}_0$	**4835.7**	5362.9 (+10.9%)	4932.8 (+2%)
$\mathcal{M}_1, \mathcal{D}_0$	**4878.4**	5541.8 (+13.6%)	5090.2 (+4.3 %)
$\mathcal{M}_0, \mathcal{D}_1$	**4877.9**	5771.8 (+18.3%)	5239.3 (+7.4%)
$\mathcal{M}_1, \mathcal{D}_1$	**4961.8**	6382.6 (+28.6%)	5588 (+12.6%)
$\mathcal{M}_0, \mathcal{D}_2$	**4820.6**	5318.3 (+10.3%)	4868.6 (+1%)
$\mathcal{M}_1, \mathcal{D}_2$	**4863.1**	5497.7 (+13%)	5023.8 (+3.3%)
$\mathcal{M}_0, \mathcal{D}_3$	**4825**	5735 (+18.9%)	5164 (+7%)
$\mathcal{M}_1, \mathcal{D}_3$	**4908.7**	6390.2 (+30.2%)	5559.7 (+13.3%)
Scenarios	Velocity error $\dot{e}$ costs		
	proposed AISMC	standard ISMC ($\bar{\beta} = 15$)	standard ISMC ($\bar{\beta} = 25$)
$\mathcal{M}_0, \mathcal{D}_0$	**10442**	12413 (+18.9%)	10890 (+4.3%)
$\mathcal{M}_1, \mathcal{D}_0$	**10636**	13016 (+22.4%)	11445 (+7.6 %)
$\mathcal{M}_0, \mathcal{D}_1$	**10611**	13626 (+28.4%)	12178 (+14.8%)
$\mathcal{M}_1, \mathcal{D}_1$	**10979**	15261 (+39%)	13307 (+21.2%)
$\mathcal{M}_0, \mathcal{D}_2$	**10360**	12207 (+17.8%)	10581 (+2.1%)
$\mathcal{M}_1, \mathcal{D}_2$	**10557**	12794 (+21.2%)	11145 (+5.6 %)
$\mathcal{M}_0, \mathcal{D}_3$	**10412**	13519 (+29.8%)	11904 (+14.3%)
$\mathcal{M}_1, \mathcal{D}_3$	**10824**	15535 (+43.5%)	13134 (+21.3%)

TABLE II
STATE VARIABLES FOR UAV EQUATIONS OF MOTION

Name	Description
p_n	North position in inertial frame
p_e	East position in inertial frame
p_d	Down position in inertial frame
u_a	Surge airspeed along in body frame
v_a	Sway airspeed in body frame
w_a	Heave airspeed in body frame
ϕ	Euler roll angle
θ	Euler pitch angle
ψ	Euler yaw (heading) angle
p	Roll rate in body frame
q	Pitch rate in body frame
r	Yaw rate in body frame

where ρ is air density and V_a is the airspeed of UAV, $C_L, C_D,$ and C_m are nondimensional aerodynamic coefficients, S is the planform area of the UAV wing, and c is the mean chord of the wing. Generally, $C_L, C_D,$ and C_m are considered uncertain because they are significantly influenced by the airfoil shape, Mach number, Reynolds number and the angle of attack. F_{lift} and F_{drag} are related to f_x and f_z through an appropriate transformation [38, Ch. 4]. Also, f_x and f_z are affected by the gravity term, and by the propulsion forces from the throttle δ_t (details not shown for lack of space).

Lateral aerodynamics include lateral force f_y, roll moment l, and yaw moment n, which can be expressed depending on the sideslip angle β, roll rate p and yaw rate r, aileron angle δ_a, and rudder angle δ_r as

$$f_y = \frac{1}{2}\rho V_a^2 S C_Y(\beta, p, r, \delta_a, \delta_r) \tag{39a}$$

$$l = \frac{1}{2}\rho V_a^2 Sb C_l(\beta, p, r, \delta_a, \delta_r) \tag{39b}$$

$$n = \frac{1}{2}\rho V_a^2 Sb C_n(\beta, p, r, \delta_a, \delta_r) \tag{39c}$$

where C_Y, C_l and, C_n are nondimensional aerodynamic coefficients, and b is the UAV wingspan. Again, the nonlinear relationships in the coefficients $C_L, C_D,$ and C_m are characterized by nonlinear functions that are subject to uncertainty.

As the dynamical equations for UAV are complex, it is customary to develop design models with significantly less mathematical complexity, but still capturing the essential behavior of the system. In accordance with the literature (details can be found in [38, Ch. 6 and 9]) the UAV dynamics are approximated with reduced-order models stemming from the design of higher level guidance strategies. The guidance models comprise an airspeed-hold loop and an altitude-hold loop. The airspeed-hold loop is represented by

$$\dot{V}_a = b_{V_a}(V_a^c - V_a) \tag{40}$$

where b_{V_a} is positive constant that depend on the implementation of the autopilot and the state estimation scheme. The altitude-hold loop is represented by

$$\ddot{h} = b_{\dot{h}}(\dot{h}^c - \dot{h}) + b_h(h^c - h) \tag{41}$$

where $b_{\dot{h}}, b_h$ are positive constants that depend on the implementation of the autopilot and the state estimation schemes.

The airspeed-hold loop and the altitude-hold loop are adopted in a so-called total energy control system (TECS) which aims to control the kinetic energy and the potential energy (this is done via a double PID loop, called TECS throttle and TECS pitch). The constants $b_{V_a}, b_{\dot{h}}, b_h$ are unknown since they depend on how low-level controllers (roll/pitch/yaw loops) have been tuned. In addition, unmodeled dynamics (e.g., couplings between velocity and altitude) will certainly arise due to the reduced-order approximation. Therefore, the fixed-wing autopilot scenario provides a challenging test case for testing the proposed methodology in PID-based loops.

The open-source SITL simulator allows to run autopilots directly on PC and test their behavior in a realistic UAV simulation environment [39]. The GUI of the simulator is shown in Fig. 4. There are three windows in the GUI, the map window showing the flight path (left), the terminal window used to type flight mode commands (upper right), and the console real-time feedback of UAV flight status parameters and wind disturbance (bottom right). Fig. 5 displays the architecture of the attitude controllers in SITL. The attitude controller modules can either
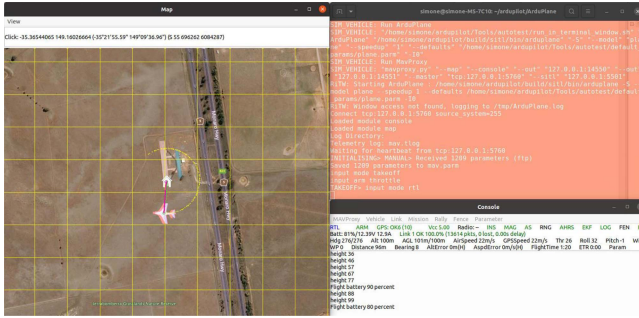
Fig. 4. GUI of ArduPlane simulator: Map window, terminal window, and console real-time window.
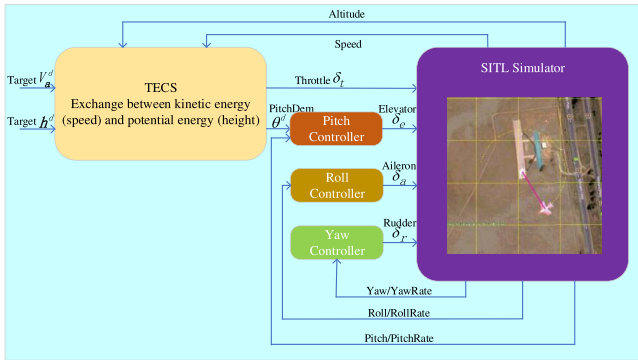

Fig. 5. Architecture of autopilot SITL set-up: TECS, roll controller, pitch controller, yaw controller, and simulator.

TABLE III
PARAMETERS SELECTION FOR THE PROPOSED AISMC METHOD IN
ARDUPILOT AUTOPILOT

Loop	$\hat{K}_i(0)$ $i = 0, 1, 2$	α_i $i = 0, 1, 2$	ϵ	η
pitch	10^{-5}	201.73	100	0.01
roll	10^{-5}	79.75	100	1.01
yaw	10^{-5}	1000	100	10^{-7}
TECS throttle	10^{-5}	0.009	100	3.3
TECS pitch	10^{-5}	1.08	100	80

contain the original cascaded PID autopilot (original ArduPilot), or a user-designed autopilot.

The original ArduPilot autopilot is used for comparison. The TECS in ArduPilot is indeed a PID loop for kinetic energy and a PID loop for potential energy. In addition, the low-level roll/pitch/yaw loops are also PID loops. All these PID loops can be modified according to the proposed theory, so that the standard ISMC approach and the proposed AISMC approach can all be used for comparison. Therefore, Υ, Ω_1, and Ω_2 in (21) are chosen as the PID gains set in the ArduPilot code [39]. The other parameters for the proposed AISMC approach are listed in Table III and $\overline{\beta}$ for the standard ISMC are chosen as $\overline{\beta} = 80$, $\overline{\beta} = 100$, $\overline{\beta} = 120$. In addition, to the purpose of validating the importance of the AISMC idea, we also implement the ASMC method recently proposed in [16]: it is clear that, due to the lack of integral action, this ASMC or any standard ASMC cannot

TABLE IV
TRACKING ERROR COSTS FOR ORIGINAL, PROPOSED AISMC AUTOPILOT,
AND AN ASMC VERSION

Mass	Original ArduPilot autopilot					
	Roll	Pitch	Yaw	TECS throttle	TECS pitch	Total
$2 \rightarrow 1$kg	1.5	2.58	3.1	21.98	4.88	34.04
2kg	1	1	1	1	1	5.0
$2 \rightarrow 4$kg	0.59	0.84	1.7	10.96	10.12	24.21

Mass	Proposed AISMC autopilot						
	Roll	Pitch	Yaw	TECS throttle	TECS pitch	Total	Improv.%
$2 \rightarrow 1$kg	1.5	2.53	3.1	10.09	5.07	**22.29**	(-34.5%)
2kg	1.0	0.98	0.96	0.63	0.87	**4.44**	(-11.2%)
$2 \rightarrow 4$kg	0.65	0.59	1.7	7.13	7.9	**17.97**	(-25.8%)

Mass	ASMC [16] autopilot						
	Roll	Pitch	Yaw	TECS throttle	TECS pitch	Total	Degrad.%
$2 \rightarrow 1$kg	2.05	7.2	3.14	15.03	8.14	35.56	(+4.5%)
2kg	2.03	4.53	0.98	27.72	1.17	36.43	(+629%)
$2 \rightarrow 4$kg	2.02	0.68	1.59	75.69	12.76	92.74	(+283%)

The improvements for AISMC (or the degradation for ASMC) in the cost are calculated with respect to the original ArduPilot.

be embedded in PID loops. Therefore, the comparisons with the ASMC will be useful to validate that the proposed AISMC framework provides a systematic way to enhance robustness and adaptation in PID-based loops.

To evaluate the performance of the proposed method in the presence of large uncertainty, we change the mass of the UAV during the flight (which can simulate a change in the payload of the UAV). The initial mass of the UAV is 2 kg: during the flight the mass can change to 1 kg (half mass), to 4 kg (double mass), or remain 2 kg. The value of the mass and their changes are uncertain, i.e., not used in the control design, which further contributes to testing robustness to uncertainty of the different autopilots. The flight tests include a take-off phase, after which the UAV should follow an orbit at constant altitude (the mass change occurs while the UAV is orbiting). In Table IV, we report the tracking error cost for different autopilots: the tracking error costs are five, one for each PID loop in the autopilot (roll, pitch, yaw, TECS throttle, TECS pitch). We use the performance of the original ArduPilot cost to normalize other error costs, so that the original ArduPilot cost is 5.0. The tracking error costs for all the five cascade loops are shown in Table IV for the original ArduPilot, the proposed AISMC and the ASMC (without integral action). The table shows that the tracking error costs of the proposed AISMC approach are consistently smaller than the original ArduPilot: the proposed method improves performance up to 11% without mass change and more than 25% in the presence of mass change. In addition, the table shows that ASMC in unsuitable for autopilot implementation because the absence of integral action makes it impossible to track appropriately the desired set points (this explains the large values of the costs at the end of Table IV).

To visualize some of the results, the experiments with half mass and double mass are collected in Figs. 6 and 7 for both the original autopilot and the proposed AISMC autopilot. As shown in Fig. 6(a) and (b) and Fig. 7(a) and (b), the proposed
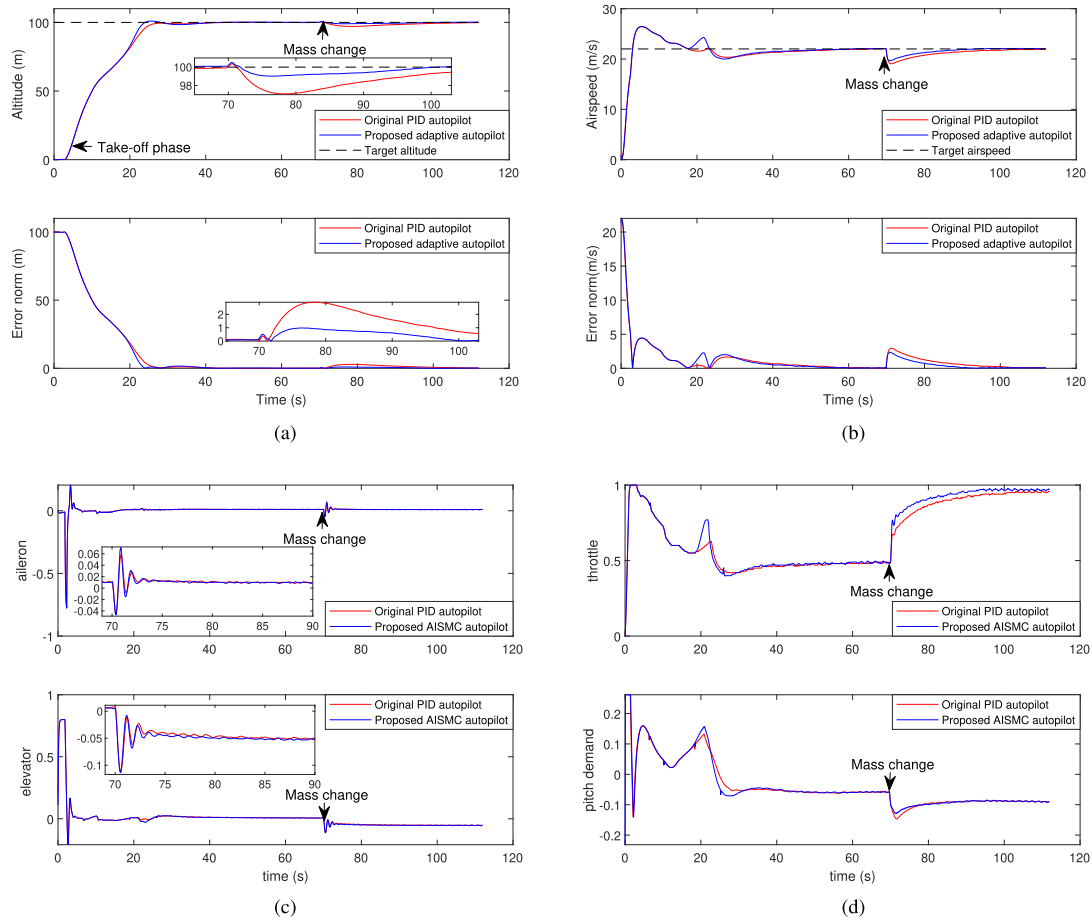
Fig. 6. UAV, mass change 2.0 kg → 1.0 kg: Comparison of original and proposed autopilot. (a) Altitude and altitude error norm. The proposed solution has negligible altitude drop after mass change. (b) Airspeed and airspeed error norm. The proposed solution converges faster to the desired airspeed after mass change. (c) Aileron and elevator. The improvements of the proposed solution are achieved with all inputs in reasonable range. (d) TECS throttle and pitch demand. The proposed solution is more reactive to mass change.

TABLE V
ALTITUDE COSTS COMPARISON FOR ORIGINAL, ADAPTIVE (AISMC, ASMC), AND NONADAPTIVE (ISMC) AUTOPILOT

Mass	AISMC (proposed)	Original ArduPilot	ISMC ($\overline{\beta} = 80$)	ISMC ($\overline{\beta} = 100$)	ISMC ($\overline{\beta} = 120$)	ASMC [16]
2 → 1kg	**0.9**	1.01	0.97	0.94	0.92	2.41
		Degrad. (+12.2%)	Degrad. (+7.8%)	Degrad. (+4.4%)	Degrad. (+2.2%)	Degrad. (+168%)
2kg	**0.87**	1	0.93	0.91	0.9	1.78
		Degrad. (+14.9%)	Degrad. (+6.9%)	Degrad. (+4.6%)	Degrad. (+3.4%)	Degrad. (+105%)
2 → 4kg	**0.9**	1.03	0.96	0.93	0.92	2.39
		Degrad. (+14.4%)	Degrad. (+6.7%)	Degrad. (+3.3%)	Degrad. (+2.2%)	Degrad. (+166%)

The percentage degradation for all autopilots is calculated with respect to the proposed AISMC.

AISMC autopilot has negligible altitude drop after mass change as compared to the original autopilot, while the airspeed is more reactive and converges faster to the desired airspeed. It is also worth mentioning that such an improved performance is achieved while all inputs are in a reasonable range: Figs. 6(d) and 7(d) show that the aileron and elevator deflections used to control the UAV all operate in the expected range (e.g., note that the elevator is maximum during take-off phase). On the

other hand, Figs. 6(c) and 7(c) report the TECS throttle and pitch demand, i.e., the set points passed to the low-level control loops: it can be seen that the demand for the proposed AISMC is more reactive during the mass change.

Finally, since the altitude is another crucial parameter to judge performance, Table V shows the altitude error costs for all six autopilots (original ArduPilot, proposed AISMC, standard ISMC with $\overline{\beta} = 80$, standard ISMC with $\overline{\beta} = 100$,
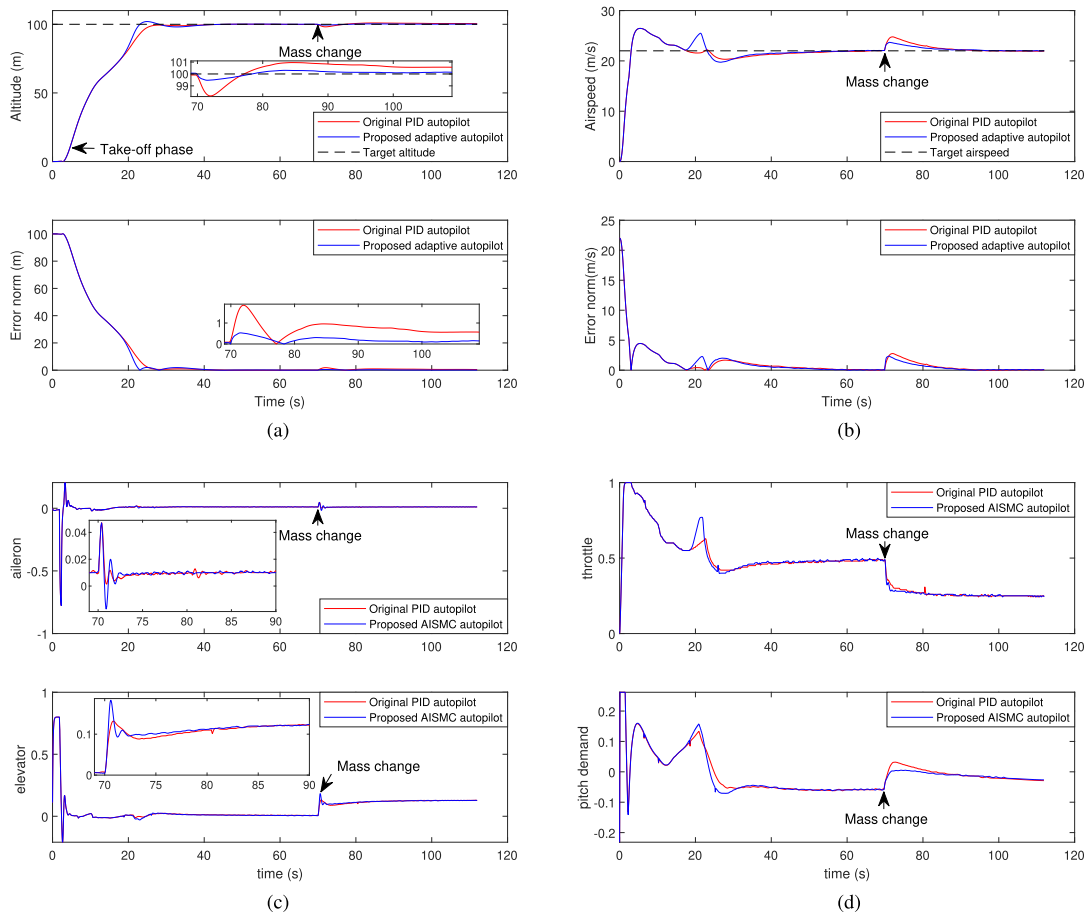
Fig. 7. UAV, mass change 2.0 kg → 4.0 kg: Comparison of original and proposed autopilot. (a) Altitude and altitude error norm. The proposed solution has negligible altitude drop after mass change. (b) Airspeed and airspeed error norm. The proposed solution converges faster to the desired airspeed after mass change. (c) Aileron and elevator. The improvements of the proposed solution are achieved with all inputs in reasonable range. (d) TECS throttle and pitch demand. The proposed solution is more reactive to mass change.

standard ISMC with $\overline{\beta} = 120$). The proposed AISMC approach has better performance than the nonadaptive ISMC, no matter how $\overline{\beta}$ is chosen. This allows to say, similar to what we have concluded in Table I for the surface vehicle, that the proposed AISMC can automatically adapt its gain for any uncertain scenario: on the other hand, the gain $\overline{\beta}$ of ISMC should be tuned appropriately.

To conclude, the proposed AISMC outperforms standard control approaches for systems with different structures (surface vehicle and aerial vehicle), and in different scenarios (with uncertain mass and uncertain mass changes).

V. CONCLUSION

This work explored a novel AISMC method with reduced *a priori* knowledge of the EL system uncertainty. We have shown that a state-dependent system uncertainty merely comes from basic properties of EL dynamics, independent of the structure of the system. It was shown that the proposed AISMC provides a systematic way to enhance robustness and adaptation in PID-based loops. Experiments on systems with different structures have been presented, i.e., surface vehicle dynamics, and SITL aerial vehicle autopilot.

A relevant future work is studying if reduced structural knowledge can be tackled even in the presence of high-order sliding mode, or in the presence of bounded inputs.

REFERENCES

[1] S. Baldi, S. Roy, and K. Yang, "Towards adaptive autopilots for fixed-wing unmanned aerial vehicles," in *Proc. 59th IEEE Conf. Decis. Control*, 2020, pp. 4724–4729.

[2] K. Shojaei, A. Kazemy, and A. Chatraei, "An observer-based neural adaptive PID^2 controller for robot manipulators including motor dynamics with a prescribed performance," *IEEE/ASME Trans. Mechatronics*, vol. 26, no. 3, pp. 1689–1699, Jun. 2021.

[3] K. Dolinský and S. Čelikovský, "Application of the method of maximum likelihood to identification of bipedal walking robots," *IEEE Trans. Control Syst. Technol.*, vol. 26, no. 4, pp. 1500–1507, Jul. 2018.

[4] M. Ye, B. D. O. Anderson, and C. Yu, "Model-independent trajectory tracking of euler-lagrange agents on directed networks," in *Proc. IEEE 55th Conf. Decis. Control*, 2016, pp. 6921–6927.

[5] C. He and J. Huang, "Leader-following consensus for multiple Euler-Lagrange systems by distributed position feedback control," *IEEE Trans. Autom. Control*, vol. 66, no. 11, pp. 5561–5568, Nov. 2021.

[6] S. Roy and S. Baldi, "A simultaneous adaptation law for a class of nonlinearly parametrized switched systems," *IEEE Control Syst. Lett.*, vol. 3, no. 3, pp. 487–492, Jul. 2019.

[7] T. L. Costa, J. C. Vendrichoski, E. S. El'Youssef, and E. R. De Pieri, "Modeling and control of an unmanned aerial vehicle with tilt rotors equipped with a camera," in *Proc. 19th Int. Conf. Adv. Robot.*, 2019, pp. 1–6.

[8] M. A. Santos, D. N. Cardoso, B. S. Rego, G. V. Raffo, and S. Esteban, "A discrete robust adaptive control of a tilt-rotor UAV for an enlarged flight envelope," in *Proc. IEEE 56th Annu. Conf. Decis. Control*, 2017, pp. 5208–5214.

[9] A. Abdessameud, A. Tayebi, and I. G. Polushin, "On the leader-follower synchronization of Euler-Lagrange systems," in *Proc. 54th IEEE Conf. Decis. Control*, 2015, pp. 1054–1059.

[10] S. Wang and J. Huang, "Adaptive leader-following consensus for multiple Euler-Lagrange systems with an uncertain leader system," *IEEE Trans. Neural Netw. Learn. Syst.*, vol. 30, no. 7, pp. 2188–2196, Jul. 2019.

[11] M. Jin, J. Lee, and N. G. Tsagarakis, "Model-free robust adaptive control of humanoid robots with flexible joints," *IEEE Trans. Ind. Electron.*, vol. 64, no. 2, pp. 1706–1715, Feb. 2017.

[12] H. Zhang, Y. Wang, Y. Wang, and J. Zhang, "A novel sliding mode control for a class of stochastic polynomial fuzzy systems based on SOS method," *IEEE Trans. Cybern.*, vol. 50, no. 3, pp. 1037–1046, Mar. 2020.

[13] M. Jin, S. H. Kang, P. H. Chang, and J. Lee, "Robust control of robot manipulators using inclusive and enhanced time delay control," *IEEE/ASME Trans. Mechatronics*, vol. 22, no. 5, pp. 2141–2152, Oct. 2017.

[14] Z. Cao, Y. Niu, and J. Song, "Finite-time sliding-mode control of Markovian jump cyber-physical systems against randomly occurring injection attacks," *IEEE Trans. Autom. Control*, vol. 65, no. 3, pp. 1264–1271, Mar. 2020.

[15] M. Van, "An enhanced robust fault tolerant control based on an adaptive fuzzy PID-nonsingular fast terminal sliding mode control for uncertain nonlinear systems," *IEEE/ASME Trans. Mechatronics*, vol. 23, no. 3, pp. 1362–1371, Jun. 2018.

[16] S. Roy, S. Baldi, and L. M. Fridman, "On adaptive sliding mode control without a priori bounded uncertainty," *Automatica*, vol. 111, 2020, Art. no. 108650.

[17] D. Y. Negrete-Chavez and J. A. Moreno, "Second-order sliding mode output feedback controller with adaptation," *Int. J. Adaptive Control Signal Process.*, vol. 30, no. 8–10, pp. 1523–1543, 2016.

[18] C. Edwards and Y. B. Shtessel, "Adaptive continuous higher order sliding mode control," *Automatica*, vol. 65, pp. 183–190, 2016.

[19] Y. B. Shtessel, J. A. Moreno, and L. M. Fridman, "Twisting sliding mode control with adaptation: Lyapunov design, methodology and application," *Automatica*, vol. 75, pp. 229–235, 2017.

[20] S. Laghrouche, M. Harmouche, F. S. Ahmed, and Y. Chitour, "Control of PEMFC air-feed system using Lyapunov-based robust and adaptive higher order sliding mode control," *IEEE Trans. Control Syst. Technol.*, vol. 23, no. 4, pp. 1594–1601, Jul. 2015.

[21] S. Roy, S. B. Roy, and I. N. Kar, "Adaptive-robust control of Euler-Lagrange systems with linearly parametrizable uncertainty bound," *IEEE Trans. Control Syst. Technol.*, vol. 26, no. 5, pp. 1842–1850, Sep. 2018.

[22] J. Khawwaf, J. Zheng, R. Chai, R. Lu, and Z. Man, "Adaptive micro-tracking control for an underwater IPMC actuator using new hyperplane-based sliding mode," *IEEE/ASME Trans. Mechatronics*, vol. 24, no. 5, pp. 2108–2117, Oct. 2019.

[23] M. P. Aghababa, "Sliding-mode control composite with disturbance observer for tracking control of mismatched uncertain nDoF nonlinear systems," *IEEE/ASME Trans. Mechatronics*, vol. 23, no. 1, pp. 482–490, Feb. 2018.

[24] V. Utkin and J. Shi, "Integral sliding mode in systems operating under uncertainty conditions," in *Proc. 35th IEEE Conf. Decis. Control*, 1996, vol. 4, pp. 4591–4596.

[25] Y. Stepanenko, Y. Cao, and C. Y. Su, "Variable structure control of robotic manipulator with PID sliding surfaces," *Int. J. Robust Nonlinear Control*, vol. 8, no. 1, pp. 79–90, 1998.

[26] D. Liu and G. Yang, "Prescribed performance model-free adaptive integral sliding mode control for discrete-time nonlinear systems," *IEEE Trans. Neural Netw. Learn. Syst.*, vol. 30, no. 7, pp. 2222–2230, Jul. 2019.

[27] M. Van, M. Mavrovouniotis, and S. S. Ge, "An adaptive backstepping nonsingular fast terminal sliding mode control for robust fault tolerant control of robot manipulators," *IEEE Trans. Syst., Man, Cybern. Syst.*, vol. 49, no. 7, pp. 1448–1458, Jul. 2019.

[28] Y. Ma, D. Li, Y. Li, and L. Yang, "A novel discrete compound integral terminal sliding mode control with disturbance compensation for PMSM speed system," *IEEE/ASME Trans. Mechatronics*, to be published, doi: 10.1109/TMECH.2021.3068192.

[29] H. Du, L. Wang, J. Chen, H. Huang, and X. Feng, "Integral sliding mode tracking control for heavy vehicle electro-hydraulic power steering system," *IEEE/ASME Trans. Mechatronics*, vol. 26, no. 3, pp. 1455–1466, Jun. 2021.

[30] J.-J. E. Slotine and M. W. Spong, "Robust robot control with bounded input torques," *J. Robot. Syst.*, vol. 2, no. 4, pp. 329–352, 1985.

[31] J. Slotine and W. P. Li, *Applied Nonlinear Control*. Englewood Cliffs, NJ, USA: Prentice-Hall, 1991.

[32] J. Song, Y. Niu, and Y. Zou, "Finite-time stabilization via sliding mode control," *IEEE Trans. Autom. Control*, vol. 62, no. 3, pp. 1478–1483, Mar. 2017.

[33] Y. Wang, B. Zhu, H. Zhang, and W. X. Zheng, "Functional observer-based finite-time adaptive ISMC for continuous systems with unknown nonlinear function," *Automatica*, vol. 125, 2021, Art. no. 109468.

[34] Q. Shen, D. Wang, S. Zhu, and E. K. Poh, "Integral-type sliding mode fault-tolerant control for attitude stabilization of spacecraft," *IEEE Trans. Control Syst. Technol.*, vol. 23, no. 3, pp. 1131–1138, May 2015.

[35] P. Li, X. Yu, Y. Zhang, and X. Peng, "Adaptive multivariable integral TSMC of a hypersonic gliding vehicle with actuator faults and model uncertainties," *IEEE/ASME Trans. Mechatronics*, vol. 22, no. 6, pp. 2723–2735, Dec. 2017.

[36] S. Roy, J. Lee, and S. Baldi, "A new adaptive-robust design for time delay control under state-dependent stability condition," *IEEE Trans. Control Syst. Technol.*, vol. 29, no. 1, pp. 420–427, Jan. 2021.

[37] H. K. Khalil, *Nonlinear Systems*. Hoboken, NJ, USA: Prentice Hall, 2002.

[38] R. W. Beard and T. W. Mclain, *Small Unmanned Aircraft Theory and Practice*. Princeton, NJ, USA: Princeton Univ. Press, 2012.

[39] "GitHub - ArduPilot/ardupilot." [Online]. Available: https://github.com/ArduPilot/ardupilot

Peng Li received the B.Sc. degree in electronic information from the Hubei University of Science and Technology, Shijiazhuang, China, in 2013, and the M.Tech. degree in electronic science and technology from the Wuhan University of Technology, Wuhan, China, in 2016. He is currently working toward the Ph.D. degree in cyber science and engineering with Southeast University, Nanjing, China.

His research interests includes adaptive nonlinear control and its applications to unmanned vehicles.

Di Liu (Member, IEEE) received the B.Sc. degree in information science from the Hubei University of Science and Technology, Shijiazhuang, China, and the M.Sc. degree in control science and engineering from the Chongqing University of Posts and Telecommunications, Chongqing, China, in 2014 and 2017, respectively, and the Ph.D. degree in cyber science and engineering from Southeast University, Nanjing, China, in 2021. She is currently working toward the second Ph.D. degree in systems and control with the Bernoulli Institute for Mathematics, Computer Science, and Artificial Intelligence, University of Groningen, The Netherlands.

Her research interests include learning systems and control, with application in intelligent transportation, automated vehicles, unmanned aerial vehicles.

Simone Baldi (Senior Member, IEEE) received the B.Sc. degree in electrical engineering, and the M.Sc. and Ph.D. degrees in automatic control engineering from the University of Florence, Florence, Italy, in 2005, 2007, and 2011, respectively.

Currently, he is a Professor with Southeast University, Nanjing, China, with a guest position at Delft Center for Systems and Control, TU Delft, the Netherlands, where he was an Assistant Professor. His research interests include adaptive and learning systems with applications in networked systems and intelligent vehicles.

Dr. Baldi was awarded outstanding reviewer of *Applied Energy* in 2016 and *Automatica* in 2017. He is the Subject Editor of *International Journal of Adaptive Control and Signal Processing* and an Associate Editor of *IEEE Control Systems Letters*.